Transport properties and equation of state for HCNO mixtures in and beyond the warm dense matter regime

Christopher Ticknor, Lee A. Collins, and Joel D. Kress

Phys. Rev. E **92**, 023101 — Published 4 August 2015

DOI: 10.1103/PhysRevE.92.023101

Transport properties and equation of state for HCNO mixtures in and beyond the Warm Dense Matter regime

Christopher Ticknor, Lee A. Collins, and Joel D. Kress
Theoretical Division, Los Alamos National Laboratory, Los Alamos, New Mexico 87545, USA

We present simulations of a four component mixture of HCNO with orbital free molecular dynamics (OFMD). These simulations were conducted for 5-200 eV with densities ranging between 0.184-36.8 g/cm^3. We extract the equation of state from the simulations and compare to average atom models. We found that we only need to add a cold curve model to find excellent agreement. Additionally, we studied mass transport properties. We present fits to the self-diffusion and shear viscosity which are able to reproduce the transport properties over the parameter range studied. We compare these OFMD results to models based on the Coulomb coupling parameter and one component plasmas.

PACS numbers: 03.75Hh,67.85-d

I. INTRODUCTION

Heterogeneity can profoundly change the behavior of a system when compared to a homogenous, single component plasma. This is particularly true at a fundamental level in high-energy density (HED) physics where mixtures of elements can lead to anomalous behavior. Good examples are found in inertial confinement fusion (ICF) experiments, where lasers compress material to extraordinary densities [1–3]. Invariably the ablator, the plastic shell holding the nuclear fuel, mixes with the fuel when imploded, changing the material properties and reducing the yield [4]. Recent studies have been designed to directly study this intriguing mixing process [5, 6]. More generally, HED mixtures are found throughout astrophysics, examples range from interiors of planets [7] to white dwarfs [8].

A full theoretical understanding of mixtures remains illusive due to the large number of phenomena that occur. One important approach has been the application of a first principles method called quantum molecular dynamics (QMD), which combines density functional theory to determine the electronic structure with the classical motion of ions [9–11]. This creates a consistent theory of HED matter that accurately produces transport properties and EOS for mixtures [12–16]. Despite QMD's success and accuracy, it is computationally intense and this limits its use. Other theories have begun to approach the challenge of mixtures from different avenues, such as generalizations of the one component plasma (OCP) model [17] such as the works of Refs. [18, 19]. Equation of states (EOSs) for mixtures has been obtained from quantum average atom methods [20–26]. Other notable recent efforts have extended such quantum average atom formulations to explicitly treat mixtures [27, 28] with the hyper-netted chain formalism.

Yet these alternative methods to first principles QMD simulations remain limited in scope. Therefore it remains important to directly study mixtures and explore and characterize their general behavior. Here we study the behavior of mixtures with a flavor of QMD, called orbital free molecular dynamic (OFMD), which uses Thomas-Fermi-Dirac theory to construct the electronic density and is valid at higher temperature (T$> 5eV$). We have performed large OFMD simulations of a representative four component mixture of Hydrogen (H), Carbon (C), Nitrogen (N) and Oxygen (O). We study densities ranging between 0.184 and 36.8 g/cm^3 and temperatures of 5 to 200 eV. This density range is representative of PBX 9501, an energetic material [29], with a compression ratio of 0.1 to 20. The molecular mixture is representative of high explosives, and it differs from the cases encountered in modeling ice-giant planets because of its much lower hydrogen content.

From these simulations we extract the EOS, self-diffusion coefficients, and the shear viscosity of the mixtures. With these results we inform and test simpler models used to produce EOS. For example, we are able to accurately reproduce the OFMD EOS with an effective average atom Thomas-Fermi-Dirac (TFD) method. Additionally, we compare the transport properties to models which use the plasma coupling parameter, Γ, to parameterize the behavior of viscosity [30] and diffusion [18, 26]. These models produce good estimates of the OFMD with more simple models.

In the remainder of the paper, we first review the OFMD simulation methods. Then we review an average atom model used to reproduce the EOS. We present the transport properties and their behavior as a function of density and temperature. Finally, we look at the results of Γ models used predict transport properties.

II. METHODS

We now review the methods we used to produce the EOS and transport properties from OFMD simulations. Additionally, we discuss other methods used to understand the transport properties of the system.

A. OFMD simulations

In this work we have performed large four-component OFMD simulations of an HCNO mixture. Throughout this paper, we will label these four component simulations and their results as 4C-OFMD. We use the Born-Oppenheimer approximation and separate the electronic and ionic degrees of freedom. For a given ion configuration, the electronic structure is found, and then classical equations of motion for the ions are numerically integrated within the isokinetic ensemble [31]. The simulation has a total number of ions: $N = \sum_\gamma N_\gamma$ where for the γ^{th} species, there are N_γ ions with nuclear charge Z_γ and atomic weight A_γ. Additionally there are $N_e = \sum_\gamma N_\gamma Z_\gamma$ electrons in the volume. The electronic density is found with a finite-temperature orbital-free density functional theory [32] treatment (Thomas-Fermi-Dirac) with the kinetic-entropic form of Perrot [33]. The electron-ion interaction is obtained from a regularization prescription [32] and the exchange-correlation from a local density Perdew-Zunger form [34]. OFMD has proven accurate for extracting equations-of-state and mass transport properties for the warm dense matter (WDM) regime and up to the dense plasmas regime [35–38].

The mixture density ranges between 0.184 and 36.8 g/cm^3 at temperatures of 5eV to 200eV. This density range is representative of PBX 9501 with a compression ratio bewtween 0.1 to 20. Typical simulations have 54 H, 31 C, 39 N, and 43 O ions (167 total ions). For the two most dilute simulations, we use 27 H, 15 C, 19 N, and 21 O ions (82 total ions). These smaller samples produce EOS and transport properties that are converged to within statistical error to a larger simulation when compared to when both are at denser conditions (0.92 g/cm^3). The simulations required a large amount of computational resources and were run on Cielo, a Cray XE6 with AMD Opterons at Los Alamos. Typical simulations ran on 4096 cores for 24-48 hours to produce 30,000 to 50,000 MD time steps. This large number of time steps was needed to converge the viscosity, which was particularly difficult for the dilute simulations.

Instead of using all four constituents, an alternative two-component model (2C-OFMD) was found to reproduce well the EOS and average transport properties. A single representative heavy ion was used in place of C, N and O; we will call this the *heavy composite* model, which will be labeled A. This composite element has an atomic mass ($A_A = \sum_{\gamma=CNO}(N_\gamma/N)\cdot A_\gamma$ ∼17.1 g/mol) and charge ($Z_A = \sum_{\gamma=CNO}(N_\gamma/N)\cdot Z_\gamma$ ∼7.1). In this manner, the number of ions can be reduced while retaining significant numbers of each ion, and thus saving computational cost while retaining or improving statistical significance of each constituent.

For the OFMD simulations, the total pressure of the system is

$$P = nk_BT + P_e(V,T). \tag{1}$$

This is the sum of the ideal gas pressure of the ions (at a constant T enforced by the isokinetic thermostat) and the electron pressure P_e, computed via the electronic forces from the OFMD trajectory and averaged after the system has equilibrated.

We extract the transport properties from the 4 component OFMD simulations [39, 40]. The self-diffusion coefficient of a particular ion species, D_γ is computed from the integral of the velocity autocorrelation function (VACF), which is:

$$D_\gamma = \frac{1}{3}\int_0^\infty \langle \vec{v}_i(t)\cdot\vec{v}_i(0)\rangle dt, \tag{2}$$

where $\vec{v}_i$ is the velocity of the i^{th} particle (γ species). The shear viscosity was computed from the autocorrelation function of the stress tensor

$$\eta = \frac{V}{k_BT}\int_0^\infty \langle P_{12}(t')P_{12}(0)\rangle dt', \tag{3}$$

for further details see [39, 41].

We use empirical fits to the integrals of the autocorrelation functions to shorten the duration of the trajectory required to converge the transport properties [37, 42]. For our set of parameters, the ACFs are generally not structured, and a simple exponential fit suffices to extract the desired properties. The statistical error inherent in computing correlation functions from molecular dynamics is estimated [43] as $\sqrt{2\tau/N_t dt}$ where $N_t dt$ is the length of the trajectory and τ is the correlation time of the ACF. We usually fit the ACF over a time interval of 0 to 4τ. The length of the simulation is much longer than τ. For the viscosity, the error computed is 10% or less for all simulations except for the two most dilute simulations, where the error is less than 18%. The error for the self-diffusion is less than 5%, due to the additional factor of $1/\sqrt{N_\gamma}$ from averaging the VACF over all of the ion of type γ.

B. Average atom Thomas-Fermi-Dirac model

An average atom (AA) Thomas-Fermi-Dirac (TFD) electronic model can be used to reasonably reproduce the thermal EOS of the 4C-OFMD simulations. The average atom model assumes a single ion of type γ has charge Z_γ and atomic mass of A_γ centered in a sphere, for which one solves for the electronic density and electrostatic potential such that there are Z_γ electrons in the spherical volume bounded by r_{ws}, the Wigner-Seitz radius. This is found from the single particle volume: $V = 4\pi r_{ws}^3/3$. More details of the average atom TFD model can be found in Ref. [44, 45].

A standard way to decompose an EOS is to consider the thermal behavior and T=0 (cold curve) behavior as separate contributions [46]. With this decomposition, the electronic pressure can be written as: $P(V,T) = P_{e0}(V) + P_e(V,T)$. Since AA TFD simulations produce the total pressure, $P(V,T)$, to obtain the

thermal electronic pressure, $P_e(V,T)$, we need to find and subtract the cold curve, $P_{e0}(V)$. In our implementation of this TFD model, we take special care to make sure that the thermodynamic properties are well behaved at each V as $T \to 0$. We set the thermal pressure to $P_e(V,T) = AT^2$ below T_{ref}. We find T_{ref} by solving $P_e(V,T_{ref})/P_{e0}(V) = 0.01$. This behavior is anticipated at low temperature from the TFD model. Additionally, this procedure is applied to energy and entropy (linear in T) and produces a thermodynamically consistent EOS and smooth thermodynamic functions and derivative with respect to both T and V of pressure, energy, and entropy as a function of both V and T.

We consider two distinct ways to apply the average atom model to represent a mixture. First an *average element model* (AE-AA), is defined where A_{av} and Z_{av} are averaged over *all* the atoms: $Z_{av} = \sum_{\gamma=HCNO}(N_\gamma/N)\cdot Z_\gamma$ ~5.13 and $A_{av} = \sum_{\gamma=HCNO}(N_\gamma/N)\cdot A_\gamma$ ~9.9 g/mol. This is straightforward and produces good results. A second more accurate model uses a 2 component model (2C-AA) utilizing the *heavy composite* ion (A) and a pressure matching mixing rule. To perform the mixing rule [41], we define the desired state: T, V, N, N_H, and N_A, and then solve for the partial volumes (V_H and V_A) at which the pressures, from H and A, are equal under the constraint that their volume sum to the total volume:

$$\begin{aligned} P_H(V_H,T) &= P_A(V_A,T) \\ V &= V_H + V_A \end{aligned} \tag{4}$$

C. Γ models

Previous work [18, 26, 30, 35, 47–49] examined transport properties of the one component plasma (OCP) as a function of $\Gamma = Z^2/(akT)$, where Z is the charge of an ion and a is the interparticle separation, both of these will be further specified below. We will compare our 4C-OFMD simulations with the models of Bastea [18], Hansen [30], and Arnault [26]. For viscosity, Bastea gives $\eta/\eta_0 = A\Gamma^{-2} + B\Gamma^{-s} + C\Gamma$ with $A = 0.482$, $B = 0.629$, $C = 0.00188$, $s = 0.878$, $\eta_0 = \rho M r_{ws}^2 \omega_p$ and $\omega_p^2 = 4\pi\rho e^2 Z^2/M$ [18]. For diffusion, we use the simple fit of Hansen to estimate the diffusion as $D/D_0 = 2.95\Gamma^{-1.34}$ with $D_0 = \omega_p a^2$ [30]. Additionally, we compare our diffusion results to [26], which uses portions of the model from Ref. [48, 49]. The Arnault model defines several different regions in Γ in which different fits are provided in each region [26].

The most successful means to estimate η and D used the effective charge of the ions. So to define Γ, Z becomes Z^*, which is a function of ρ and T. It should be clear that Z^* is not the total charge of an ion but its effective charge in dense plasma environment. In Fig. 1 the effective charge for H, A (CNO composite), and the average element (av) are shown as a function of temperature for three densities: 0.184 (black dotted line), 1.84 (red dashed line) and 18.4 (blue line) g/cm^3. For high density the Z^* changes (solid blue) only a little and for low density (black dashed), the Z^* changes the most, starting the lowest and finishing the highest for each atom.

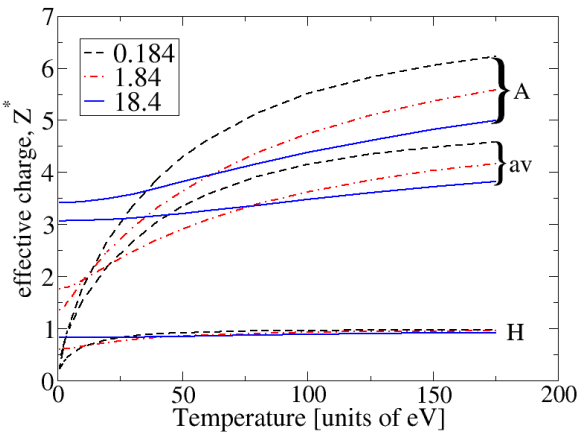

FIG. 1: (color online) The effective charge for H, A (CNO composite) and av (average element) as a function of temperature for three densities: 0.184 (black dotted line), 1.84 (red dashed line) and 18.4 (blue line) g/cm^3.

To use the Γ model to find η and diffusion we use $a = r_{ws}^{av}$ and the average ion mass, M_{av}, to define both η_0 and Γ. Here r_{ws}^{av} and M_{av} are found by using the average element's properties. For the viscosity, we use the average element effective charge, Z_{av}^* [16]. For diffusion, we find both D_H and D_A by using Z_H^* and Z_A^* [16] while satisfying Eq. (4). This procedure gives good results for both diffusion and viscosity as will be shown below.

III. COMPARISON OF AVERAGE ATOM TFD TO OFMD

Here we compare the 4C-OFMD EOS to the inexpensive AA-TFD models. To do this directly, we decompose the EOS into the thermal behavior and cold curve, as discussed above. Each of the models has its own unique cold curve behavior. Every TFD model has a critical volume [50] where the exchange term pulls the electron density out of the interstitial regions. This includes the 4C-OFMD and results in the cold curve pressure being zero. The AE-AA model gives a unique critical volume. The 2C-AA has two distinct critical volumes, one for H and one for A (CNO composite). Here it makes sense to construct a cold curve model. Finally, the 4C-OFMD give another distinct result due to the many-particle nature of the OFMD result. Therefore to quantitatively compare the electronic EOS from 4C-OFMD simulations and the average atom TFD model, we must model the cold curve to add this to the average atom model. The model we use for the OFMD cold curve is:

$$\begin{aligned} P_{e0} &= A(\rho-\rho_0)^2\Theta(\rho-\rho_0) \\ P_e^{TFD}(\rho,T) &+ P_{e0}(\rho) = P_e^{OFMD}(\rho,T) \end{aligned} \tag{5}$$

where $\Theta(x)$ is the Heaviside function and is equal to 1 when $x \geq 0$ and 0 otherwise.

It should be noted that we are seeking to compare the thermal behavior of the 4C-OFMD and the AA models. Generally, TFD models do not correctly predict the cold curve behavior of a material in the dilute limit. The comparison of the thermal behavior can be done, as we have in Eq. (5), by adding the cold curve to the AA results, or it can be done by subtracting it from the OFMD result. We chose to add it, so it can more easily be visualized in Fig. 2.

We perform a least-squares fit to determine A and ρ_0 directly comparing the average atom plus the cold curve model to the 4C-OFMD data; we used the relative error so not to over-emphasize the high temperature data. For the 2C-AA, we find A =40.946 GPa/(g/cm^3)^2 and ρ_0=0.4435 g/cm^3. For the average atom TFD model, we find A =41.421 GPa/(g/cm^3)^2 and ρ_0=0.646 g/cm^3.

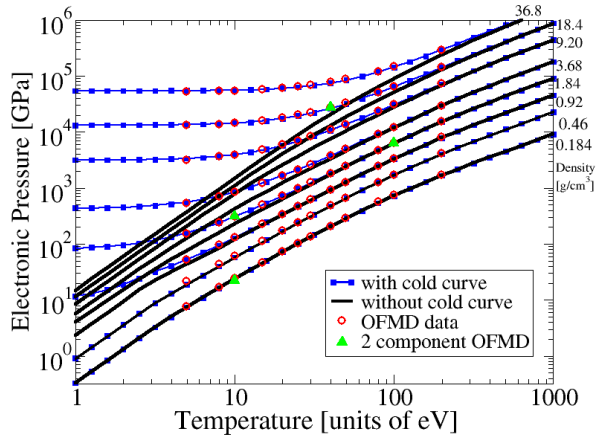

FIG. 2: (color online) The electronic pressure as a function of temperature at several different densities. 4C-OFMD results (red circles) as a function of temperature at various densities. For the AE-AA, the EOS is shown without (black) and with (blue squares) the modified cold curve model. The agreement with the 4C-OFMD is excellent. For all data points, the average relative error is 1.5% . 2C-OFMD simulations are shown as green triangles at select locations.

The electronic pressure from the 4C-OFMD simulations and the 2C-AA model with a cold curve are shown in Fig. 2. The red circles are from 4C-OFMD simulations, the black lines are from the 2C-AA model, P_e^{TFD}, and the blue lines with squares include the cold curve, $P_e^{TFD} + P_{e0}$. We see excellent agreement between the OFMD simulations and 2 component average atom model with the cold curve. For the 2C-AA, the results have a relative chi-squared of 0.05, and the average error is 1.5%. The largest disagreement is near the transition where $P_{e0} \rightarrow 0$ as temperature goes to zero for a density of 0.46 g/cm^3. Beside these points, the agreement is excellent. The results from the average atom model are slightly higher in pressure than the 2 component average atom, particularly at low T. The relative chi-squared is 0.28 and the average error is 5 %. For the most dilute 4-OFMD simulations, the cold curve is zero, i.e. $\rho < \rho_0$, and the agreement with the mixed average atom model is very good.

We find that the 2C-AA model reproduces the 4C-OFMD pressure more accurately because it allows the H and the heavy ions to take up different volumes. This is particularly important in the dilute limit. For example in the low T limit, the H component of the gas occupies much more volume. In the most dilute case, the volume occupied by the H is 19% then lowers to 7% as temperature is increased. In contrast at the highest compression ratio, the volume of H is roughly constant starting at 9% and lowering to 7%. The 7% number is the ideal gas limit (each electron takes up equal volume and 7% of the electrons are from H), and this is why all the high temperature results trend to it.

IV. TRANSPORT PROPERTIES OF HCNO MIXTURES

A. Viscosity

We now examine the shear viscosity of the HCNO mixture. In Fig. 3(a) we show the viscosity for the 4C-OFMD simulations as a function of temperature for three densities (g/cm^3): 0.184 (black dots), 1.84 (red squares) and 18.4 (blue triangle). In all cases, the viscosity increases as temperature increases, scaling like an plasma. We first see that the density significantly affects the temperature dependence of the viscosity. At highest density, the temperature dependence is much weaker. For example at high density and low temperature, below $T \sim$ 30eV, the viscosity becomes nearly temperature independent. For higher densities (36.8 g/cm^3, not shown) the viscosity actually increases as temperature is decreased, scaling like a liquid metal. For the low density simulations, the viscosity goes up more rapidly compared to more dense systems as temperature is increased.

We now rescale the viscosity to see if we can obtain a single functional form to describe all of the data. This work is inspired by the idea of universal transport properties [51–53]. We have found that rescaling the viscosity as

$$\bar{\eta} = \eta \rho^{1/5} / T^{5/2} \tag{6}$$

works well if we fit $\bar{\eta}$ to a function $exp[ax + bx^2]$ where $x = \ln[\rho/T^3]$. In Eq. (6), the $T^{5/2}$ is reminiscent of the Braginskii form of viscosity for fully ionized plasmas [54]. This form gives a reasonable fit to the data as shown in Fig. 3 (b). The parameters a and b are found by a least squares fit to all of the 4C-OFMD data: a=0.900614 and b=0.0172519. This fit for the viscosity reproduces 87 of the 96 data points to within 50%. An example of an outlying data point, in fact the worst example, is at 8eV and 0.184g/cm^3. The fit to Eq. (6) is shown in Fig. 3

(a). The rescaled data fit has an average relative error of 22%.

In Fig. 3 (c), we present the rescaled viscosity as a function of Γ. The viscosity model of Bastea [18] does not reproduce the viscosity as well as the fit we present, Eq. (6). In particular, at high density the Bastea model typically over estimates the viscosity, but otherwise gives good estimates, with an average relative error of 39%.

B. Diffusion

In Fig. 4 we show the self-diffusion coefficients for the 4C-OFMD simulations as a function of temperature for all ions at 1.84 g/cm^3. There is clearly a different temperature dependence for the heavy ions: C (green dotted), N (blue dash dot), and O (violet dashed), when compared to the H (black dots). The temperature dependence of D_H is slightly above linear while D_A is just below linear. We see that C (green dotted) is beginning to deviate from N (blue dash dot) and O (violet dash). But overall this shows that the behavior of C, N, and O are similar over the range studied.

To further the analysis, we will look at an averaged two component system and analyze the behavior. We average the self-diffusion coefficients of C, N, and O into a single value, labeled A (CNO composite). In Fig. 4 we show the A diffusion coefficient as red-squares. Additionally, the self-diffusion from the 2C-OFMD simulations (green triangles) agree well with A (CNO composite). We will now look at the temperature dependence of the self-diffusion with the simple form $D = cT^\nu$ for three example densities. The results for 0.184, 1.84, (shown in Fig. 4), and 18.4 g/cm^3 are shown in Table I. As density increases, so

density [g/cm^3]	ν_H	ν_A
0.184	1.21	0.65
1.84	1.25	0.72
18.4	1.34	0.95

TABLE I: The temperature dependence (T^ν) of self-diffusion coefficients of both H and A for three densities.

does the temperature scaling of the diffusion. Additionally, while the temperature dependence of H is larger, it does not increase as much as the temperature dependence of A as density is increased.

To estimate the diffusion, we have rescaled the data like the viscosity, but we found that a consistently better result comes from the Γ models [26, 30]. We will now compare the OFMD data against such models. In Fig. 5 (a) and (b), we show the 4C-OFMD self-diffusion coefficient (+) with the self-diffusion coefficient predicted by [30] (squares). Each plot shows three different densities 0.184 (black), 1.84 (red), and 18.4 g/cm^3 (blue). We see generally good agreement. For the dilute example, the black squares are systematically lower than the OFMD data (+). In contrast, at high density the blue squares are systematically higher than the OFMD data (+). In Fig. 5 (b), a noticeable deviation is at low T and high density, where the Γ fit results in predictions that become too small as T is lowered.

In Fig. 5 (c) the rescaled diffusion coefficients are shown as a function of Γ, H (blue squares) and A (red dots), and are compared to the Γ models of Refs. [26, 30]. The agreement with [30] is quiet remarkable with an average relative error of 20% for D_H and 16% for D_A. Compared to the viscosity Γ models, Γ spans a much larger range, due to the smaller Z^* of H and larger Z^* of A. Furthermore, we see good agreement generally except when Γ is small ($\Gamma < 0.1$) and large ($\Gamma > 10$). In both cases, the OFMD data is larger than the estimate.

We have also included the model from Ref. [26] (green dashed), which uses portions of the model from Ref. [48, 49]. The Arnault model has an average relative error of 48% for D_H and 26% for D_A. The most significant disagreement for D_H occurs at low Γ where the model becomes much larger than the data. Similarly the 4C-OFMD data is becoming larger than the Hansen fit, just not at the rate of the Arnault model. At moderate $\Gamma \sim 1$, the Arnault model goes below the data. At large Γ, the Arnault model result does a good job of capturing the deviation of the data from the Hansen model. Since these models are based on the OCP, so we do not expect perfect agreement.

V. CONCLUSION

In this work, we presented large OFMD simulations for a four component mixture of HCNO. Our simulations covered densities of 0.184 to 36.8 g/cm^3 with temperature ranging from 5 to 200 eV. From these simulations, we studied both the temperature and density dependence of the EOS, self-diffusion coefficients, and shear viscosity.

In addition to the 4C-OFMD simulations, we found that we could replace the four component mixture with an effective two component mixture, (2C-OFMD), where the heavy ions were averaged into a single composite element. This simplified model reproduced the EOS, shear viscosity, and self diffusion coefficients with good accuracy.

We compared the EOS obtained from the 4C-OFMD to a commonly used TFD average atom model. We found excellent agreement once we added a cold curve model to the 2C-AA, (Fig. 2). In the 2C-AA model, we pressure matched the H ion and the A ion (CNO composite) under the constraint of additive volumes. This model was superior to the the average element model (AE-AA) which uses a single HCNO composite ion to model the whole system.

We looked at the transport properties of the HCNO mixture. Several examples of viscosity and self-diffusion were given as a function of both density and temperature. We have found that rescaling the viscosity (Eq. 6) and fitting to a simple function, we were to reproduce the 4C-

OFMD data well. Additionally, the viscosity was also compared to the Γ based model of Bastea. The self-diffusion coefficients are shown in Figs. 4 and 5. In Fig. 5, we compared the 4C-OFMD results and predictions of diffusion coefficients for both H and A (CNO composite) using effective single component Γ models of Refs. [26, 30]. We found these to be good estimates of the self-diffusion coefficients.

This work will also pave the way forward on the interiors of white dwarfs with compositions such as C, O, and Fe [8]. Future work will be to study mixtures with a larger difference in Z, for example H-Ag. Additionally, comparisons to orbital based quantum models which can handle mixtures, such as Refs [27, 28], should be made. Any difference found on the comparisons will illuminate the path for improving the models.

Acknowledgments

The authors are acknowledge illuminating discussions with E. Meyer and J. Coe. The authors gratefully acknowledge support from ASC, computing resource from CCC, and LANL which is operated by LANS, LLC for the NNSA of the U.S. DOE under Contract No. DE-AC52-06NA25396.

[1] R. F. Smith, J. H. Eggert, R. Jeanloz, T. S. Duffy, D. G. Braun, J. R. Patterson, R. E. Rudd, J. Biener, A. E. Lazicki, A. V. Hamza, et al., Nature **511**, 330 (2014).

[2] A. L. Kritcher, T. Döppner, D. Swift, J. Hawreliak, G. Collins, J. Nilsen, B. Bachmann, E. Dewald, D. Strozzi, S. Felker, et al., High Energy Density Physics **10**, 27 (2014), URL http://www.sciencedirect.com/science/article/pii/S1574181813001894.

[3] L. B. Fletcher, A. L. Kritcher, A. Pak, T. Ma, T. Döppner, C. Fortmann, L. Divol, O. S. Jones, O. L. Landen, H. A. Scott, et al., Phys. Rev. Lett. **112**, 145004 (2014), URL http://link.aps.org/doi/10.1103/PhysRevLett.112.145004.

[4] S. W. Haan, J. D. Lindl, D. A. Callahan, D. S. Clark, J. D. Salmonson, B. A. Hammel, L. J. Atherton, R. C. Cook, M. J. Edwards, S. Glenzer, et al., Physics of Plasmas (1994-present) **18**, 051001 (2011), URL http://scitation.aip.org/content/aip/journal/pop/18/5/10.1063/1.3592169.

[5] V. A. Smalyuk, R. E. Tipton, J. E. Pino, D. T. Casey, G. P. Grim, B. A. Remington, D. P. Rowley, S. V. Weber, M. Barrios, L. R. Benedetti, et al., Phys. Rev. Lett. **112**, 025002 (2014), URL http://link.aps.org/doi/10.1103/PhysRevLett.112.025002.

[6] D. T. Casey, V. A. Smalyuk, R. E. Tipton, J. E. Pino, G. P. Grim, B. A. Remington, D. P. Rowley, S. V. Weber, M. Barrios, L. R. Benedetti, et al., Physics of Plasmas (1994-present) **21**, 092705 (2014), URL http://scitation.aip.org/content/aip/journal/pop/21/9/10.1063/1.4894215.

[7] T. Montmerle, J.-C. Augereau, M. Chaussidon, M. Gounelle, B. Marty, and A. Morbidelli, Earth, Moon, and Planets **98**, 39 (2006), ISSN 0167-9295, URL http://dx.doi.org/10.1007/s11038-006-9087-5.

[8] D. Koester, *White Dwarf Stars* (Springer, Netherlands, 2013), ISBN 978-94-007-5614-4, URL http://dx.doi.org/10.1007/978-94-007-5615-1_11.

[9] D. Marx and J. Hutter, *Modern Methods and Algorithms of Quantum Chemistry* (John von Neumann Institute for Computing, Julich, Germany, 2000).

[10] A. E. Mattsson, P. A. Schultz, M. P. Desjarlais, T. R. Mattsson, and K. Leung, Modelling and Simulation in Materials Science and Engineering **13**, R1 (2005).

[11] J. Clerouin, E. L. Pollock, and G. Zerah, Phys. Rev. A **46**, 5130 (1992), URL http://link.aps.org/doi/10.1103/PhysRevA.46.5130.

[12] T. R. Mattsson, J. M. D. Lane, K. R. Cochrane, M. P. Desjarlais, A. P. Thompson, F. Pierce, and G. S. Grest, Phys. Rev. B **81**, 054103 (2010), URL http://link.aps.org/doi/10.1103/PhysRevB.81.054103.

[13] S. X. Hu, T. R. Boehly, and L. A. Collins, Phys. Rev. E **89**, 063104 (2014), URL http://link.aps.org/doi/10.1103/PhysRevE.89.063104.

[14] R. J. Magyar, S. Root, K. Cochrane, T. R. Mattsson, and D. G. Flicker, Phys. Rev. B **91**, 134109 (2015), URL http://link.aps.org/doi/10.1103/PhysRevB.91.134109.

[15] F. Lambert, J. Clérouin, J.-F. Danel, L. Kazandjian, and G. Zérah, Phys. Rev. E **77**, 026402 (2008), URL http://link.aps.org/doi/10.1103/PhysRevE.77.026402.

[16] F. Lambert and V. Recoules, Phys. Rev. E **86**, 026405 (2012), URL http://link.aps.org/doi/10.1103/PhysRevE.86.026405.

[17] M. Baus and J.-P. Hansen, Physics Reports **59**, 1 (1980), ISSN 0370-1573, URL http://www.sciencedirect.com/science/article/pii/0370157380900228.

[18] S. Bastea, Phys. Rev. E **71**, 056405 (2005), URL http://link.aps.org/doi/10.1103/PhysRevE.71.056405.

[19] J. Daligault, Phys. Rev. Lett. **108**, 225004 (2012), URL http://link.aps.org/doi/10.1103/PhysRevLett.108.225004.

[20] G. Massacrier, A. Y. Potekhin, and G. Chabrier, Phys. Rev. E **84**, 056406 (2011), URL http://link.aps.org/doi/10.1103/PhysRevE.84.056406.

[21] B. Wilson, V. Sonnad, P. Sterne, and W. Isaacs, Journal of Quantitative Spectroscopy and Radiative Transfer **99**, 658 (2006), ISSN 0022-4073, radiative Properties of Hot Dense Matter, URL http://www.sciencedirect.com/science/article/pii/S0022407305001846.

[22] J. Pain, High Energy Density Physics **3**, 204 (2007), ISSN 1574-1818, radiative Properties of Hot Dense Matter, URL http://www.sciencedirect.com/science/article/pii/S1574181807000316.

[23] B. F. Rozsnyai, High Energy Density Physics **10**, 16 (2014), ISSN 1574-1818, URL http://www.sciencedirect.com/science/article/pii/S1574181813001882.

[24] C. Blancard and G. Faussurier, Phys. Rev. E **69**,

016409 (2004), URL http://link.aps.org/doi/10.1103/PhysRevE.69.016409.

[25] G. Faussurier, C. Blancard, P. Coss, and P. Renaudin, Physics of Plasmas (1994-present) **17**, 052707 (2010), URL http://scitation.aip.org/content/aip/journal/pop/17/5/10.1063/1.3420276.

[26] P. Arnault, High Energy Density Physics **9**, 711 (2013), URL http://www.sciencedirect.com/science/article/pii/S1574181813001651.

[27] C. E. Starrett and D. Saumon, Phys. Rev. E **87**, 013104 (2013), URL http://link.aps.org/doi/10.1103/PhysRevE.87.013104.

[28] C. E. Starrett, D. Saumon, J. Daligault, and S. Hamel, Phys. Rev. E **90**, 033110 (2014), URL http://link.aps.org/doi/10.1103/PhysRevE.90.033110.

[29] T. R. Gibbs and A. Popolato, eds., *LASL Explosive Property Data* (University of California Press, 1980).

[30] J. P. Hansen, G. M. Torrie, and P. Vieillefosse, Phys. Rev. A **16**, 2153 (1977), URL http://link.aps.org/doi/10.1103/PhysRevA.16.2153.

[31] P. Minary, G. J. Martyna, and M. E. Tuckerman, The Journal of Chemical Physics **118**, 2510 (2003), URL http://scitation.aip.org/content/aip/journal/jcp/118/6/10.1063/1.1534582.

[32] F. Lambert, J. Clérouin, and G. Zérah, Phys. Rev. E **73**, 016403 (2006), URL http://link.aps.org/doi/10.1103/PhysRevE.73.016403.

[33] F. Perrot, Phys. Rev. A **20**, 586 (1979), URL http://link.aps.org/doi/10.1103/PhysRevA.20.586.

[34] J. P. Perdew and A. Zunger, Phys. Rev. B **23**, 5048 (1981), URL http://link.aps.org/doi/10.1103/PhysRevB.23.5048.

[35] J. D. Kress, J. S. Cohen, D. A. Horner, F. Lambert, and L. A. Collins, Phys. Rev. E **82**, 036404 (2010), URL http://link.aps.org/doi/10.1103/PhysRevE.82.036404.

[36] J. D. Kress, J. S. Cohen, D. P. Kilcrease, D. A. Horner, and L. A. Collins, Phys. Rev. E **83**, 026404 (2011), URL http://link.aps.org/doi/10.1103/PhysRevE.83.026404.

[37] D. A. Horner, J. D. Kress, and L. A. Collins, Phys. Rev. B **77**, 064102 (2008), URL http://link.aps.org/doi/10.1103/PhysRevB.77.064102.

[38] D. A. Horner, F. Lambert, J. D. Kress, and L. A. Collins, Phys. Rev. B **80**, 024305 (2009), URL http://link.aps.org/doi/10.1103/PhysRevB.80.024305.

[39] M. P. Allen and D. J. Tildesley, *Computer Simulations of Liquids* (Oxford University Press, 2009).

[40] D. Alfè and M. J. Gillan, Phys. Rev. Lett. **81**, 5161 (1998), URL http://link.aps.org/doi/10.1103/PhysRevLett.81.5161.

[41] L. Burakovsky, C. Ticknor, J. D. Kress, L. A. Collins, and F. Lambert, Phys. Rev. E **87**, 023104 (2013), URL http://link.aps.org/doi/10.1103/PhysRevE.87.023104.

[42] E. R. Meyer, J. D. Kress, L. A. Collins, and C. Ticknor, Phys. Rev. E **90**, 043101 (2014), URL http://link.aps.org/doi/10.1103/PhysRevE.90.043101.

[43] R. Zwanzig and N. K. Ailawadi, Phys. Rev. **182**, 280 (1969), URL http://link.aps.org/doi/10.1103/PhysRev.182.280.

[44] A. F. Nikiforov, V. G. Novikov, and V. B. Urarov, *Quantum-Statistical Models of Hot Dense Matter* (Birkhauser, Basel, 2005).

[45] P. Fromy, C. Deutsch, and G. Maynard, Physics of Plasmas **3**, 714 (1996), URL http://scitation.aip.org/content/aip/journal/pop/3/3/10.1063/1.871806.

[46] S. P. Lyon and J. D. Johnson, Los Alamos National Laboratory Tech. Rep **LA-UR-92-3407** (1992).

[47] J. G. Clearouin, M. H. Cherfi, and G. Zerah, EPL (Europhysics Letters) **42**, 37 (1998), URL http://stacks.iop.org/0295-5075/42/i=1/a=037.

[48] J. Daligault, Phys. Rev. Lett. **96**, 065003 (2006), URL http://link.aps.org/doi/10.1103/PhysRevLett.96.065003.

[49] J. Daligault, Phys. Rev. Lett. **103**, 029901 (2009), URL http://link.aps.org/doi/10.1103/PhysRevLett.103.029901.

[50] S. Eliezer, A. Ghatak, and H. Hora, eds., *Fundamentals of Equations of State* (World Scientific Pub Co Inc, 2002).

[51] M. Dzugutov, Nature **381**, 137 (1996).

[52] Y. Rosenfeld, Journal of Physics: Condensed Matter **11**, 5415 (1999), URL http://stacks.iop.org/0953-8984/11/i=28/a=303.

[53] Y. Fomin, V. Brazhkin, and V. Ryzhov, JETP Letters **95**, 320 (2012), ISSN 0021-3640, URL http://dx.doi.org/10.1134/S0021364012060045.

[54] J. Lyman Spitzer, *Physics of Fully Ionized Gases* (Dover Publications, Inc, 1990).

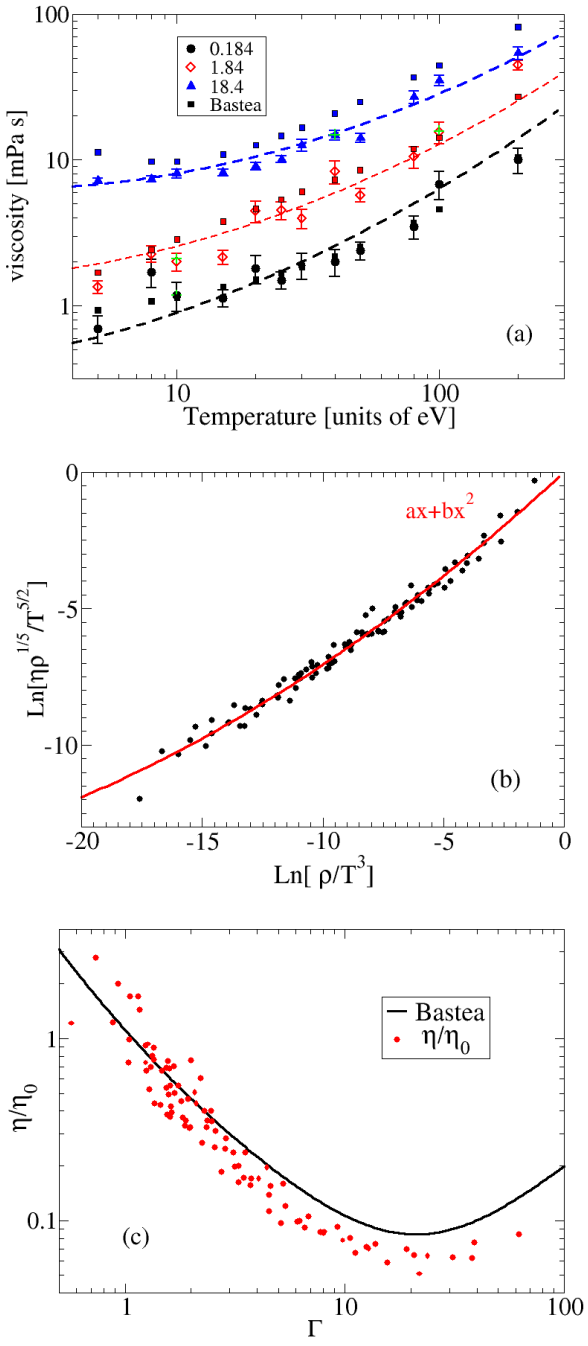

FIG. 3: (color online) (a) The 4C-OFMD simulations of viscosity as a function of temperature at three densities: 0.184 (black circles), 1.84 (red diamonds) and 18.4 (blue trinagles) g/cm^3. A few 2C-OFMD simulations are shown as green +. The colored squares are from the model of Bastea [18]. (b) The ln-ln plot of the rescaled 4C-OFMD viscosity. (c) η/η_0 shown as a function of Γ and the model from [18].

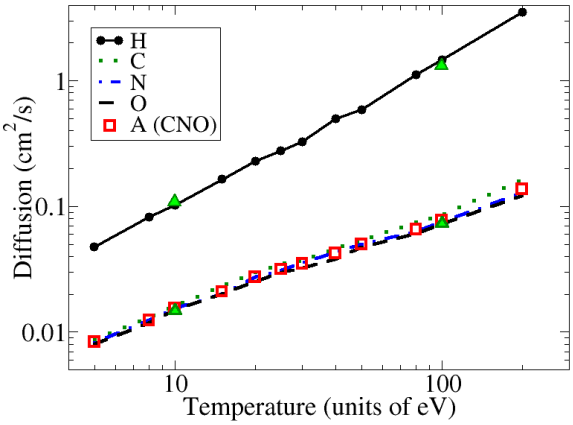

FIG. 4: (color online) The 4C-OFMD simulations of self-diffusion of the H (black dots), C (green dotted), N (blue dash dot), O (violet dashed), and the averaged 4C-OFMD result: A (red squares, CNO composite) as a function of temperature for 1.84 g/cm^3. The green triangles are self-diffusion coefficeints from the 2C-OFMD simulations.

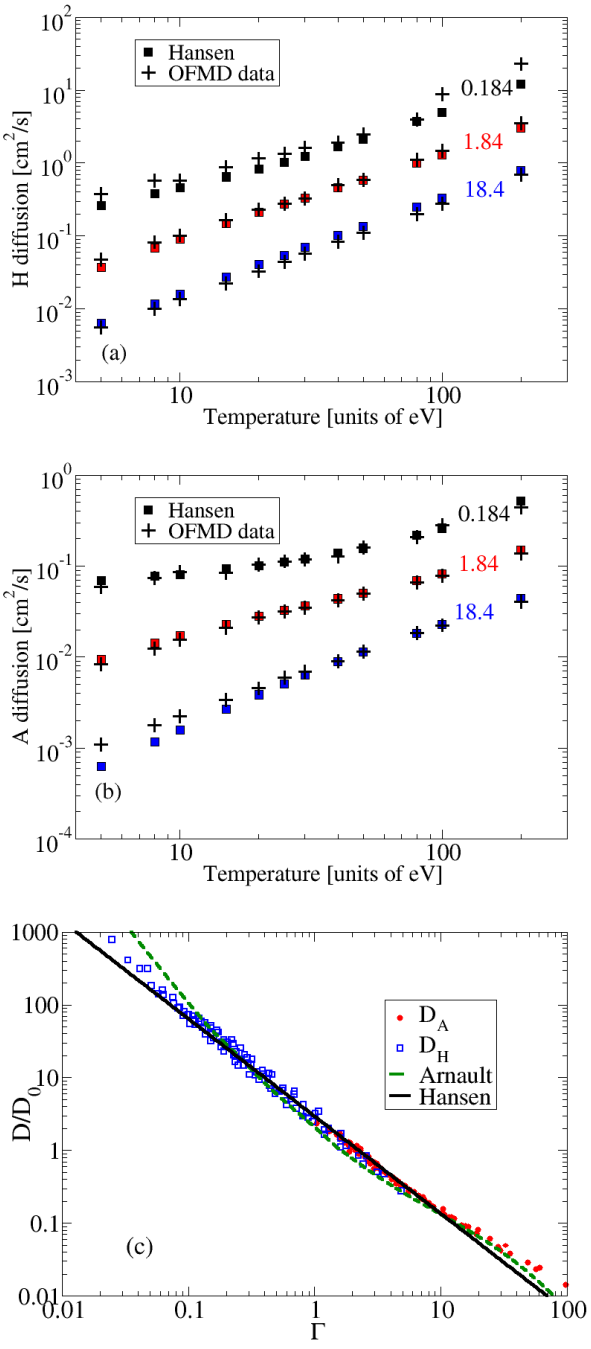

FIG. 5: (color online) The 4C-OFMD simulations of self diffusion (+) of the (a) H and (b) A (CNO composite) as a function of temperatures at three densities: 0.184 (top), 1.84 (red), and 18.4 (blue) g/cm^3. The squares are the estimates from Ref. [30], see text for details. (c) 4C-OFMD simulations of D/D_0 shown as a function of Γ for H (blue squares) and A (red dots) with models from Hansen [30] (black line) and Arnault [26] (green dashed).